

INDUSTRY ARTICLE

Stator current identification in generator among single and composite faults composed by static air-gap eccentricity and rotor inter-turn short circuit

Yu-Ling He¹  | Ming-Hao Qiu¹ | Meng-Ya Jiang¹ | Fu-Cheng Zhou¹ |
David Gerada² | Xiao-Chen Zhang² | Xiao-Dong Du³

¹Department of Mechanical Engineering, Hebei Key Laboratory of Electric Machinery Health Maintenance and Failure Prevention, North China Electric Power University, Baoding, China

²Department of Electrical and Electronics Engineering, University of Nottingham, University Park, Nottingham, UK

³State Grid Hebei Electric Power Research Institute, Shijiazhuang, China

Correspondence

Fu-Cheng Zhou, Department of Mechanical Engineering, Hebei Key Laboratory of Electric Machinery Health Maintenance and Failure Prevention, North China Electric Power University, Baoding 071003, China.
Email: zfc_01@163.com

Funding information

National Natural Science Foundation of China, Grant/Award Numbers: 51777074, 52177042

Abstract

In this study, a fault diagnosis model based on magnetic density is proposed to analyse the current characteristics of synchronous generator rotor inter-turn short circuit and air gap eccentric single fault and composite fault. The model considers the influence of rotor inter-turn short circuit and air gap eccentricity on air gap magnetic density. According to two main factors, the short circuit turns and eccentric distance, are used to reflect the short circuit and eccentricity of the generator. The detailed parameter input model of the generator can easily and quickly predict the development trend of these current parameters based on the air gap magnetic density. And the phase current is selected as the current parameter. The validity of the proposed model is verified by two-dimensional finite element analysis and experimental research.

KEYWORDS

composite fault, rotor inter-turn short circuit, static air-gap eccentricity, stator current, turbo-generator

1 | INTRODUCTION

Static air gap eccentricity (SAGE) and rotor inter-turn short circuit (RISC) are common faults of steam turbine generators [1, 2]. After the study, when the degree of SAGE is greater than 10%, will cause the violent vibration of the generator. As the failure worsened, such faults will cause the stator core deformation, winding damage and other accidents [3–5]. When the rotor inter-turn short circuit develops to a certain extent, the excitation current will increase significantly, the winding temperature increases, the reactive power decreases, the bearing vibration increases, and even lead to grounding failure, making the rotor magnetized, and the neck and shaft will be

burned when severe [6, 7]. In view of the serious consequences of these two faults and the high maintenance costs later on, scholars attach great importance to the monitoring and diagnosis of these two faults.

At present, the research of generator SAGE and RISC has many results. In terms of SAGE, document [8–14] is representative: Guerrero J.H.C et al. diagnose the SAGE of the generator based on the current value and voltage value of the generator. Min-Fu Hsieh et al. use finite element analysis (FEA) to simulate the torque of the SAGE of small permanent magnet wind turbines. Ilamparithi T et al. propose a method based on current feature analysis, which can be used to detect SAGE. Tenhunen A et al. propose a new pulse

Abbreviations: FEA, finite element analysis; MFD, magnetic flux density; MMF, magnetomotive force; PPUA, permeance per unit area; RISC, rotor inter-turn short circuit; SAGE, static air-gap eccentricity.

This is an open access article under the terms of the Creative Commons Attribution-NonCommercial-NoDerivs License, which permits use and distribution in any medium, provided the original work is properly cited, the use is non-commercial and no modifications or adaptations are made.

© 2022 The Authors. *IET Electric Power Applications* published by John Wiley & Sons Ltd on behalf of The Institution of Engineering and Technology.

method to study the harmonic distribution of the flux density under SAGE. Wang L et al. propose the application of the Maxwell stress tensor method to calculate the unbalanced magnetic tension due to SAGE, which greatly simplifies the computational difficulty and is applied in real engineering. Zarko D et al. use FEA to calculate the unbalanced magnetic tension due to SAGE, which is suitable for load and empty loads. V. Climente-Alarcon et al. obtained the stator current, voltage, or electromotive potential of the generator under the SAGE fault.

In terms of RISC, as early as 1952, A. W. W. Cameron used the non-destructive test method of winding impedance estimation to identify and diagnose the inter-turn and inter-femoral short circuit of the water turbine generator [15]. Since then, the research on the electrical parameters of the generator RISC fault, such as stator voltage, current and winding impedance, has been widely carried out [16, 17]. D. R. Albright et al. monitor the RISC using the magnetic density change rate of the air gap [18]. Cuevas et al. studied the vibration law under the generator RISC fault, and determined the short circuit degree by comparing the normal and failed vibration signals [19]. In ref. [20], the author has proposed the RISC model for studying the electromechanical parameters in synchronous generators. The advantage of the model is that both RISC and SAGE are taken into account. Moreover, the phase current and the electromagnetic torque are studied in detail in this paper. Hao L et al more accurately obtained the value of parallel branch circulation value of stator winding under different short circuit degrees by quantitative research, and verified the accuracy of the proposed model through experiments [21]. G. J. Li et al analyzed the trend of generator excitation current and output current when RISC failure occurred in the generator [22].

The existing literature lays a good foundation for the monitoring and identification of these two kinds of faults. However, none of these documents consider the combination of SAGE and RISC fault (two faults occur at the same time). In fact, because most generators have SAGE to varying degrees, when the RISC occurs again, the motor is actually in the state of composite fault of SAGE and RISC, considering only a single typical fault is incomplete in the actual operation state of the motor. The existing literature finds that the circulation characteristics of the stator parallel branch under the composite fault [23] and the resulting fixed and rotor vibration characteristics are different from that of a single fault [24, 25]. In ref. [26], the paper proposes a novel hybrid model for analysing the electromechanical characteristics under stator inter-turn short-circuit fault in synchronous generators. In refs. [27, 28], many scholars have explained the diagnosis system under single fault.

Therefore, the difference of fault characteristics of the key parameters, such as stator current, under a single and composite fault, is conducive to the rapid identification and effective diagnosis of fault components, and realize the accurate control of faults.

This paper starts with the difference of magnetic flux density (MFD) between single faults and composite faults. The analysis of the SAGE and RISC components on the

magnetomotive force (MMF) and permeance per unit area (PPUA). Furthermore, the difference of the external stator current characteristics of the generator is deduced and analysed. It is verified by Maxwell simulation and experiments to complement the existing criterion system.

2 | THEORETICAL MODEL

2.1 | Influence of RISC on MFD

The MFD of the generator is obtained by multiplying the MMF by the PPUA.

$$B(\alpha_m, t) = f(\alpha_m, t)\Lambda(\alpha_m, t) \quad (1)$$

where f is the MMF and Λ is the PPUA. The radial eccentricity of the air gap mainly affects the MFD by affecting the PPUA, while the RISC mainly affects the MFD by affecting the MMF. The following is a specific analysis.

2.2 | Influence of SAGE on PPUA

PPUA is inversely proportional to the radial air gap length:

$$\Lambda(\alpha_m, t) = \frac{\mu_0}{g_0(\alpha_m, t)} \quad (2)$$

The air gap magnetic field is symmetrically distributed when the generator is in normal operation, as shown in Figure 1a. After the static eccentricities of the air gap, the rotor centre is somewhat offset relative to the stator centre, as shown in Figure 1b.

The g_0 is average length of radial air-gap, δ_s is the relatively static air-gap eccentricity, and α_m is the mechanical circumferential angle. Based on Figure 1, the radial air gap length of the generator can be expressed as:

$$g(\alpha_m, t) = \begin{cases} g_0 \cdots \cdots \cdots \text{Normal} \\ g_0(1 - \delta_s \cos \alpha_m) \cdots \cdots \text{SAGE} \end{cases} \quad (3)$$

From Equation (3) to Equation (2) and expanding by power series, the PPUA is:

$$\Lambda(\alpha_m, t) = \begin{cases} \mu_0/g_0 = \Lambda_0 \cdots \cdots \cdots \text{Normal} \\ \Lambda_0(1 + \delta_s \cos \alpha_m + \delta_s^2 \cos^2 \alpha_m + \cdots) \\ \approx \Lambda_0(1 + \delta_s \cos \alpha_m + 0.5\delta_s^2 + +0.5\delta_s^2 \cos 2\alpha_m) \cdots \text{SAGE} \end{cases} \quad (4)$$

As can be seen from Equation (4), the SAGE will increase the PPUA of the air gap: the eccentric constant term has more $0.5\delta_s^2$ greater than zero, which is equivalent to the overall

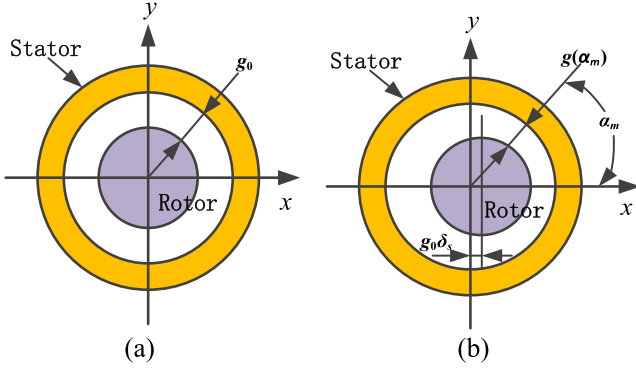


FIGURE 1 Air-gap of generator: (a) normal and (b) Static air gap eccentricity (SAGE).

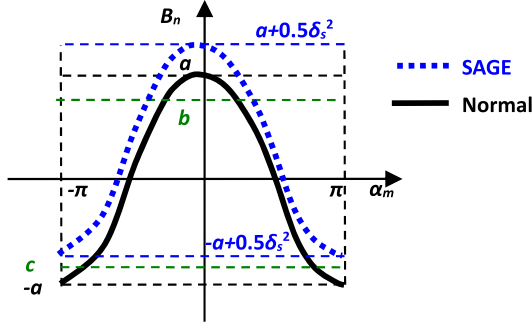


FIGURE 2 Effect of eccentricity on magnetic density.

upward translation of the air gap, resulting in the maximum and overall MFD, as shown in Figure 2.

2.3 | Influence of RISC on MMF

After the RISC, the number of the short circuit decreases and the MFD is asymmetric. Due to the decrease of the number of

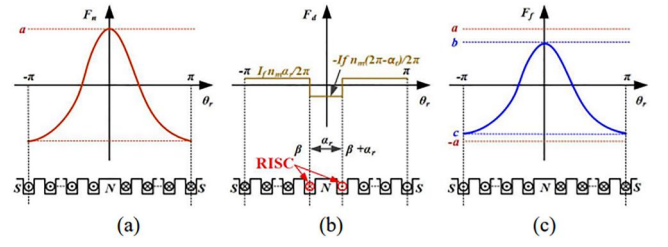


FIGURE 3 Magnetomotive force (MMF) before and after short circuit: (a) normal rotor MMF, (b) reversed MMF by RISC, and (c) rotor MMF in rotor inter-turn short circuit (RISC) case.

turns, the terminal voltage and output of the generator will be reduced.

The RISC can be regarded as applying a reverse current to offset the effect of the short circuit turn part. The main MMF of the air gap before and after the short circuit is shown in Figure 3.

According to the Gaussian magnetic flux theorem, the additional MMF generated by the short circuit turn current (see Figure 3b) can be expressed as:

$$F_d(\theta_r) = \begin{cases} \frac{I_f n_m (2\pi - \alpha_r)}{2\pi} \dots \beta' \leq \theta_r \leq \beta' + \alpha_r \\ \frac{I_f n_m \alpha_r}{2\pi} \dots \text{Other situations} \end{cases} \quad (5)$$

The I_f is the excitation current. n_m is the short circuit turns. θ_r is the circumferential angle of the rotor surface. $\alpha_m \in (0, \pi)$ is the mechanical circumferential angle. β' is the groove position angle of the short circuit turns.

Expand the additional MMF for the Fourier series available:

$$\begin{cases} F_d(\theta_r) = A_0 + \sum_{n=1}^{\infty} [A_n \cos(n\theta_r) + B_n \sin(n\theta_r)] \\ A_0 = \frac{1}{2\pi} \int_0^{2\pi} F_d(\theta_r) d\theta_r = 0 \\ A_n = \frac{1}{\pi} \int_0^{2\pi} F_d(\theta_r) \cos(n\theta_r) d\theta_r = -\frac{I_f n_m [\sin(n(\alpha_r + \beta')) - \sin(n\beta')]}{n\pi} \\ B_n = \frac{1}{\pi} \int_0^{2\pi} F_d(\theta_r) \sin(n\theta_r) d\theta_r = \frac{I_f n_m [\cos(n(\alpha_r + \beta')) + \cos(n\beta')]}{n\pi} \end{cases} \quad (6)$$

The expression of MMF after RISC is:

$$f(\alpha_m, t) = \begin{cases} \sum_{n=1}^{\infty} F_n \cos(n\omega t - p\alpha_m) \cdots \cdots \cdots \text{Normal} \\ \sum_{n=1}^{\infty} F_n \cos(n\omega t - p\alpha_m) - \sum_{m=1}^{\infty} F_{dm} \cos(m\omega t - p\alpha_m) \cdots \cdots \text{RISC} \end{cases} \quad (7)$$

F_n is the n harmonic potential amplitude. F_{dm} is the m harmonic potential amplitude generated by the short circuit turns. n is odd from 1 and m is all natural numbers from 1.

As can be seen from Equation (7). Under the normal circumstances, the MMF of the generator only has each odd harmonic, after the RISC fault occurs, each even harmonic will be added on the basis of the original odd harmonic. Macroscopically, the overall amplitude of the MMF will decrease due to the decrease of the effective turns after the short circuit, as shown in Figure 3c. As for the harmonic components, with the aggravation of the short circuit degree, the odd harmonic of the air gap will decrease and the even harmonic will increase. From the perspective of energy migration, it can be understood as: (1) the total energy of the conversion is reduced due to the short circuit factor. (2) the energy originally concentrated in the odd harmonic is partially transferred to the even harmonic due to the short circuit reason.

2.4 | Influence of composite fault on MFD

The composite fault includes the SAGE and RISC components, which will affect the PPUA and MMF. Finally, they affect the MFD. By the combination of Equations (4) and (7) into Equation (1), the MFD under each working condition is:

Based on Equation (8), combined with the above analysis, we can obtain:

- (1) The SAGE will increase the MFD, the magnetic dense harmonic composition remains unchanged, and the amplitude of each odd harmonic will increase.
- (2) Under the RISC, the MFD amplitude decreases, and the MFD harmonic component will increase except the original odd harmonic. As the short circuit intensifies, the amplitude of odd harmonic component decreases and the amplitude of even harmonic component increases.
- (3) Under the composite fault, the SAGE and RISC have the opposite impact on the magnetic density amplitude, so when comparing the composite fault and normal conditions, the change of odd harmonic amplitude of MFD should be determined according to the specific parameters, while the amplitude of even harmonic components increases. When the eccentric is certain, the odd harmonic magnetic compact amplitude of the composite fault decreases compared with the SAGE fault, but the even harmonic amplitude increases. If the short circuit is the same, the magnetic dense odd harmonic and even harmonic amplitude increase compared with the RISC fault.

2.5 | Analysis of phase current under single and composite faults

According to Faraday's law of electromagnetic induction and the expression formula of phase current is:

$$I(\alpha_m, t) = \frac{B(\alpha_m, t) l v}{Z} = \frac{B(\alpha_m, t) l \pi R_s n}{30Z} \quad (9)$$

The l is the axial length of stator core, generally approximately equal to the axial length of the stator core. v is the linear

$$B(\alpha_m, t) = \begin{cases} \sum_{n=1}^{\infty} F_n \cos(n\omega t - p\alpha_m) \Lambda_0 \cdots \cdots \cdots \text{Normal} \\ \sum_{n=1}^{\infty} F_n \cos(n\omega t - p\alpha_m) \Lambda_0 (1 + \delta_s \cos \alpha_m + 0.5\delta_s^2 + 0.5\delta_s^2 \cos 2\alpha_m) \\ \cdots \cdots \cdots \text{SAGE} \\ \left[\sum_{n=1}^{\infty} F_n \cos(n\omega t - p\alpha_m) - \sum_{m=1}^{\infty} F_{dm} \cos(m\omega t - p\alpha_m) \right] \Lambda_0 \cdots \cdots \text{RISC} \\ \left[\sum_{n=1}^{\infty} F_n \cos(n\omega t - p\alpha_m) - \sum_{m=1}^{\infty} F_{dm} \cos(m\omega t - p\alpha_m) \right] \\ \times \Lambda_0 (1 + \delta_s \cos \alpha_m + 0.5\delta_s^2 + 0.5\delta_s^2 \cos 2\alpha_m) \cdots \cdots \text{Combined fault} \end{cases} \quad (8)$$

rotating velocity of air-gap magnetic field. R_s is the inner diameter of the stator core, n is the rotor speed. Z is the stator winding reactance.

As can be seen from Equation (9), the change of stator current mainly depends on the change of MFD and the change of rotational speed, and the other parameters are fixed values. Since the SAGE and the RISC between the rotor are small, the speed is assumed to remain constant for analysis. In this way, the current change trend is consistent with the change trend of MFD:

- (1) Under the SAGE fault, the stator current increases slightly, and the amplitude of each odd harmonic wave increases slightly.
- (2) Under the RISC fault, the stator current decreases, the odd harmonic component decreases, but the even harmonic component increases.
- (3) The comparison between current and normal conditions under composite fault depends on the relative degree of

SAGE and RISC. Under the same eccentric, the composite fault harmonic amplitude and harmonic amplitude of odd harmonic amplitude are less than a single eccentric fault, but the even harmonic amplitude is greater than a single eccentric fault. Under the same short circuit, the composite fault current amplitude and odd harmonic amplitude are greater than a single short circuit.

3 | FEA AND EXPERIMENTAL VALIDATION

3.1 | FEA and experimental setup

This prototype generator is specifically designed and manufactured ourselves and is able to simulate RISC and SAGE. This paper establishes FEA model in ANSYS Maxwell according to the CS-5 hidden pole synchronous generator design

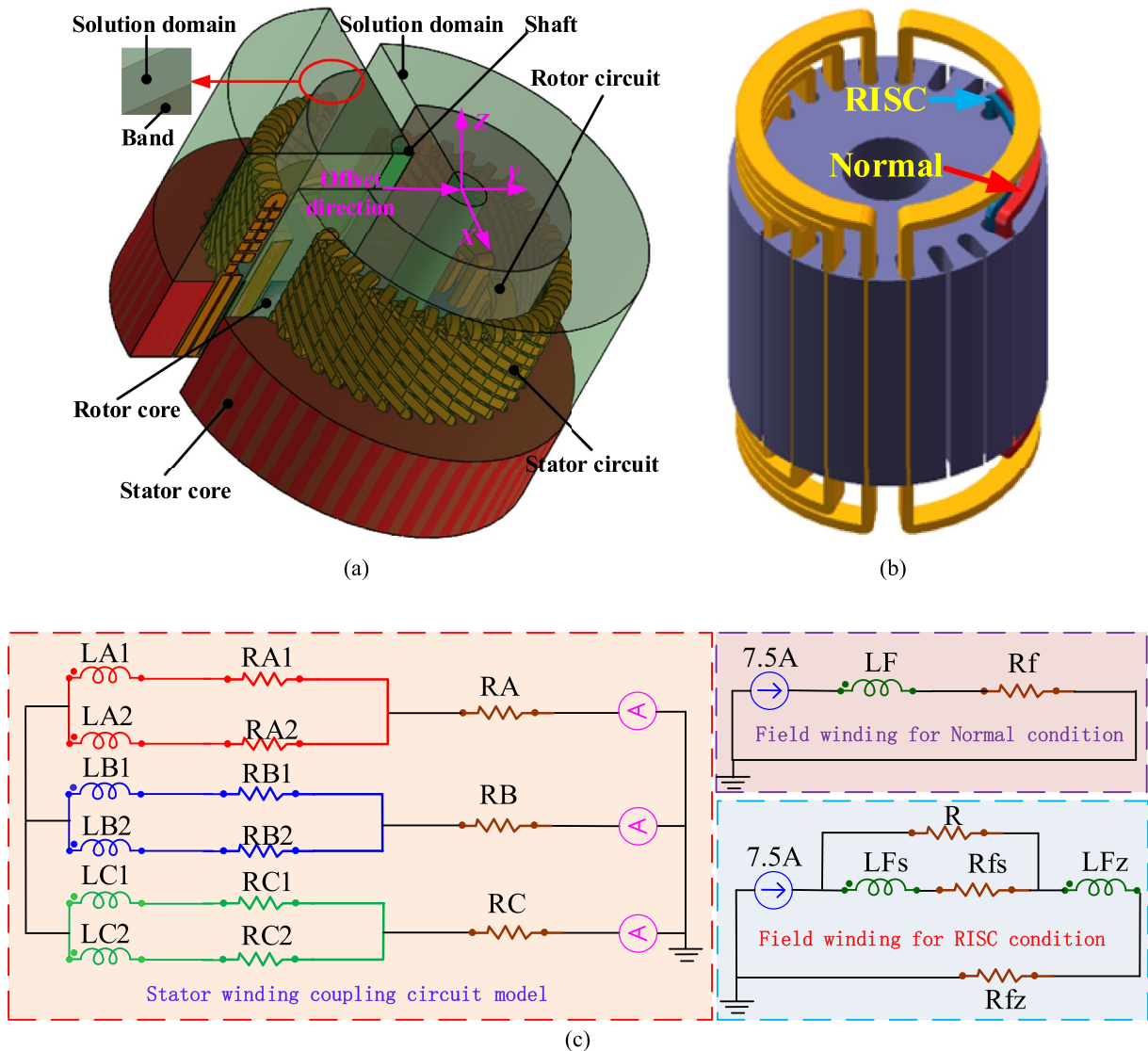


FIGURE 4 Finite element model setup: (a) Static air gap eccentricity (SAGE) model, (b) rotor inter-turn short circuit (RISC) model, and (c) external coupling circuit model.

parameters, and verifies the stability and convergence of the model through previous calculations. Parameters are listed in Table 1.

This paper adopts the 3D model of FEA. Since this paper is an experimental simulation of the generator set, it cannot reach the actual production capacity of the generator set. Therefore, the method used in this paper is to connect the load box and the output terminal of the generator set, and adjust the resistance value of the resistance box to the full-load operation state of the generator to obtain more realistic phase current data.

TABLE 1 Key parameters of analysis generators

Parameters	Values	Parameters	Values
Rated power	5 kVA	Outer diameter of stator	250.5 mm
Rated voltage	380 V	Inner diameter of stator	145 mm
Rated rotating speed	3000 rpm	Stator core length	130 mm
Rated power factor	0.8	Outer diameter of rotor	142.6 mm
Radial air-gap length	1.2 mm	Pole-pairs	1
Stator slots	36	Parallel branches	2

The ANSYS Electromagnetics was used in the simulation section. The simulation method for simulation fault is as follows:

- (1) SAGE fault: This is achieved by modifying the physical model so that the rotor core and the excitation winding are offset by a certain distance relative to the stator core in the horizontal direction. As shown in Figure 4a, the eccentric is 0.1 and 0.2 mm respectively, and the relative eccentricity is 8% and 17% respectively.
- (2) RISC fault: Firstly, to reasonably simulate the short circuit behaviours, the section of the short circuit winding bar is divided into two components in 3D model. One is to represent the short circuit part and the other is to represent the normal part, as shown in Figure 4b. Then by setting the short circuit winding LF's turns and the unshort circuit part winding LFz turns in the outer circuit coupled to the physical model (the number of turns is the total turns where the short circuit is located), also changing the resistance values R_{fs} and R_{fz} of the short circuit and unshort partial winding, the sum of both is always the total resistance value R_f for normal operation, as shown in Figure 4c. This paper simulates 5% and 10% of the two interop short circuit conditions. Air gap eccentric fault and rotor short circuit fault do not affect the stator winding

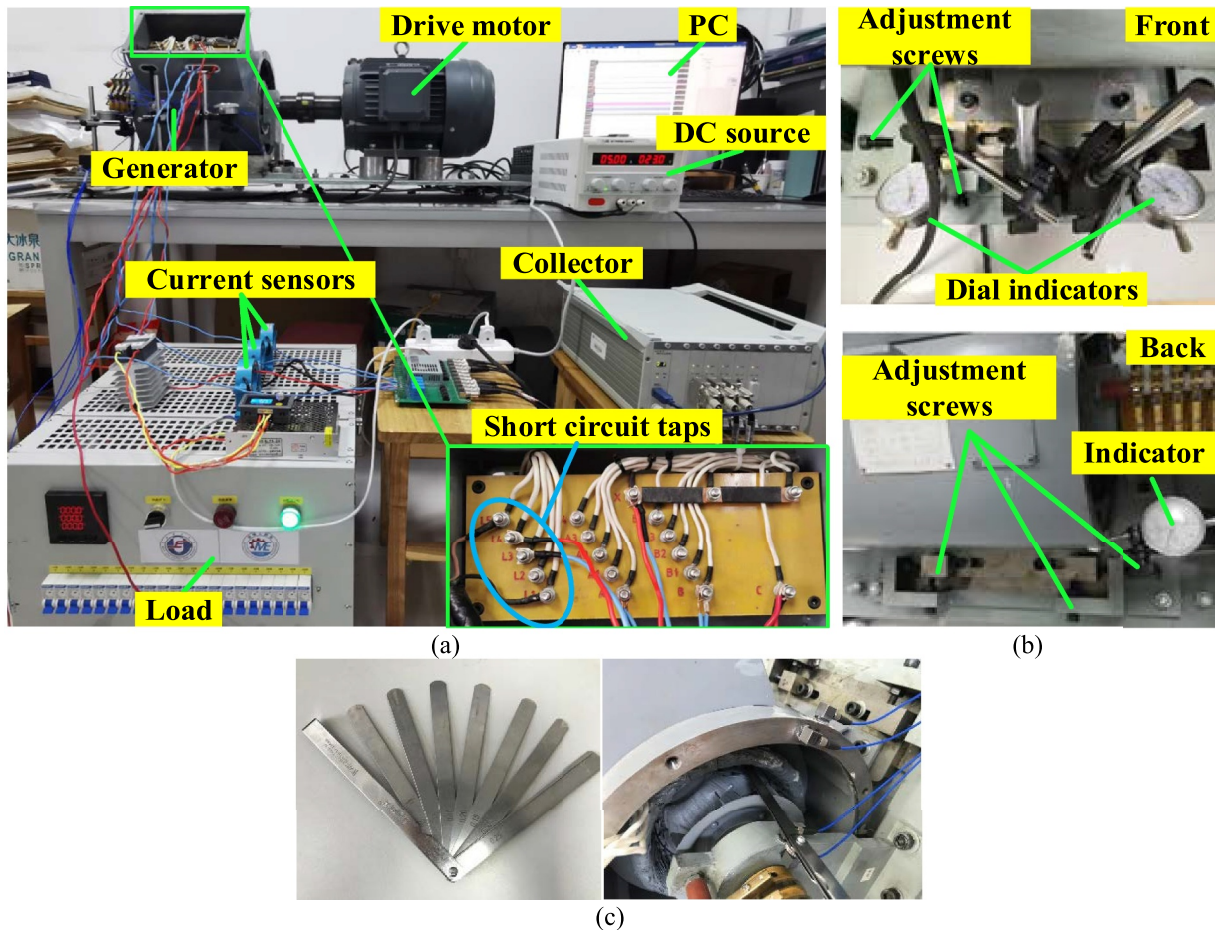


FIGURE 5 CS-5 fault simulating prototype generator: (a) general outlook, (b) setting air gap width, and (c) measuring air gap width.

coupling circuit setting, the circuit is consistent before and after the fault, as shown in Figure 4c.

- (3) Composite fault: perform the above (1) and (2) operations at the same time.

During the simulation, the band speed was set to 3000 rpm, starting at 0 s, termination at 0.04 s and step at 0.0002 s, that is, the sampling harmonic was 5000 Hz.

Experimental by CS-5 fault simulation generator is shown in Figure 5a. The setting method of each fault is as follows:

- (1) SAGE fault: The rotor is kept stable to the foundation by the bearing blocks, while the stator can be moved along both the horizontally radial direction and the axial direction. The radial movement of the stator can be performed through 4 screws (two on the front side and 2 on the back side) and controlled by two dial indicators. In the meantime, the axial movement of the stator can be also performed by another 4 screws (2 on the left side and 2 on the right side) and controlled by another 2 dial indicators.

In this paper, we only discuss the radial SAGE. To reduce the errors, a group of high precision gauges are employed to check the air-gap length and compared with the values indicated in the dial indicators.

The generator stator can be set by horizontal radial and axial displacement of the left and right rotor. The offset is

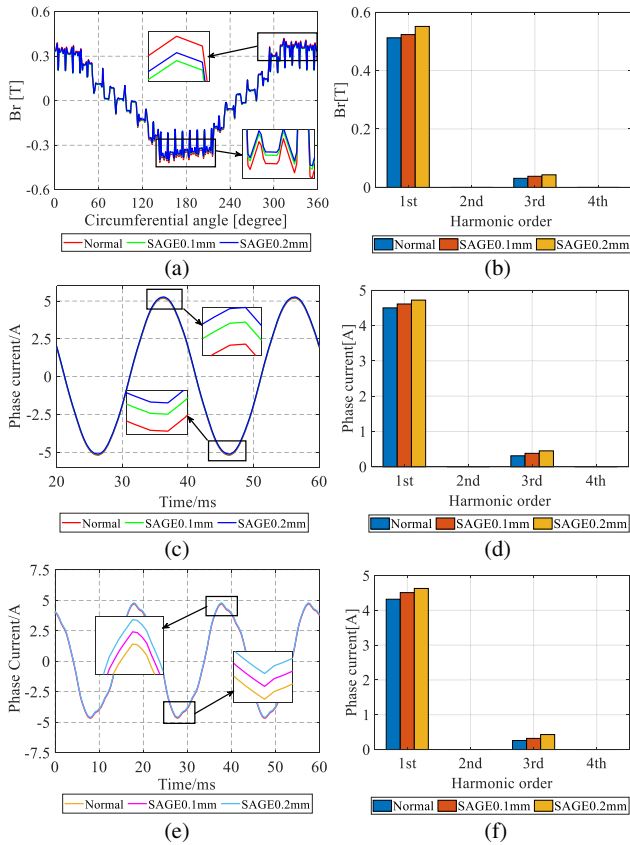


FIGURE 6 Magnetic flux density (MFD) and phase current variation before and after static air-gap eccentricity.

measured by the micrometre. As shown in Figure 5b, and the eccentricity value is verified by high precision plug gauge, as shown in Figure 5c. During the experiment, 0.1 and 0.2 mm radial static eccentric was set respectively, and the relative eccentricity was 8% and 17%.

- (2) RISC fault: The generator is equipped with a circuit panel, including 0% (L1), 5% (L2), 10% (L3), 15% (L4), 100% (L5), as shown in Figure 5a. During the experiment, 5% (L1-L2) and 10% (L1-L3) were set respectively.
- (3) Composite fault: perform the above (1) and (2) operations at the same time.

3.2 | Results and discussion

3.2.1 | MFD and current change after SAGE failure

The FEA results of the MFD change of the generator before and after the SAGE are shown in Figure 6a,b, and the FEA and experimental results of the stator phase current change are shown in Figure 6c,d and Figure 6e,f.

As can be seen from Figure 6, the change trend of MFD and current under the SAGE is basically the same. The SAGE

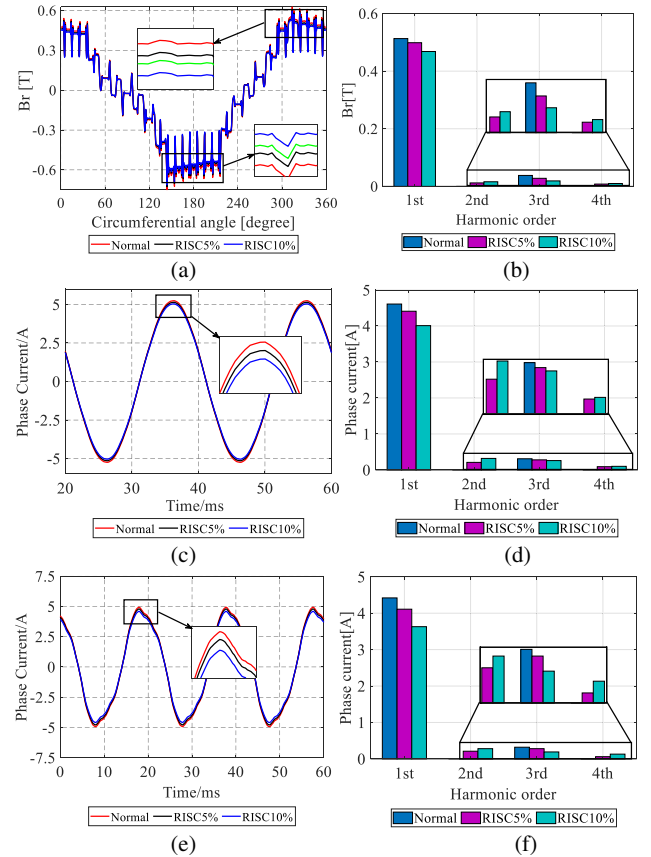


FIGURE 7 Magnetic flux density (MFD) and phase current variation before and after rotor inter-turn short circuit (RISC).

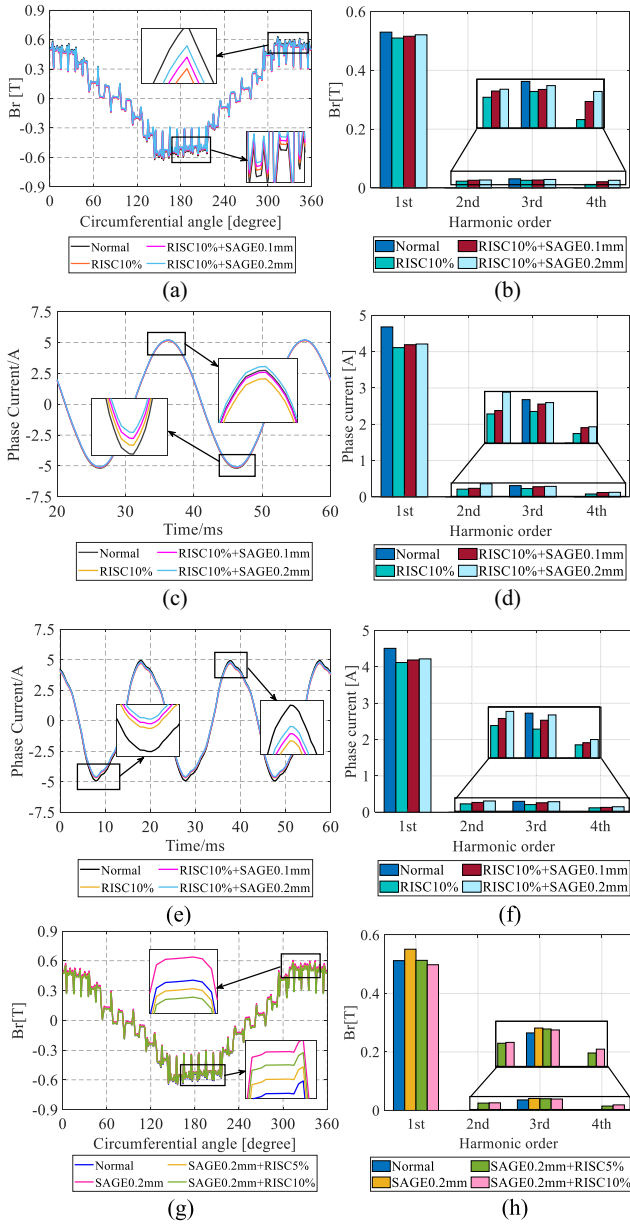


FIGURE 8 Magnetic flux density (MFD) and phase current variation before and after eccentricity/short circuit increment under composite faults.

will increase the MFD amplitude and odd harmonic amplitude, and the MFD and current waveform show the overall upward translation trend, and the larger the eccentric value, the more the MFD and current increase and the more upward translation of the waveform. This result is consistent with the theoretical analysis obtained in Figure 2.

3.2.2 | MFD and current change after SAGE and RISC growth under compound fault

The FEA and experimental results of generator MFD and stator current change before and after short circuit are shown in Figure 7a,b. As can be seen from Figure 7a,b, the MFD and

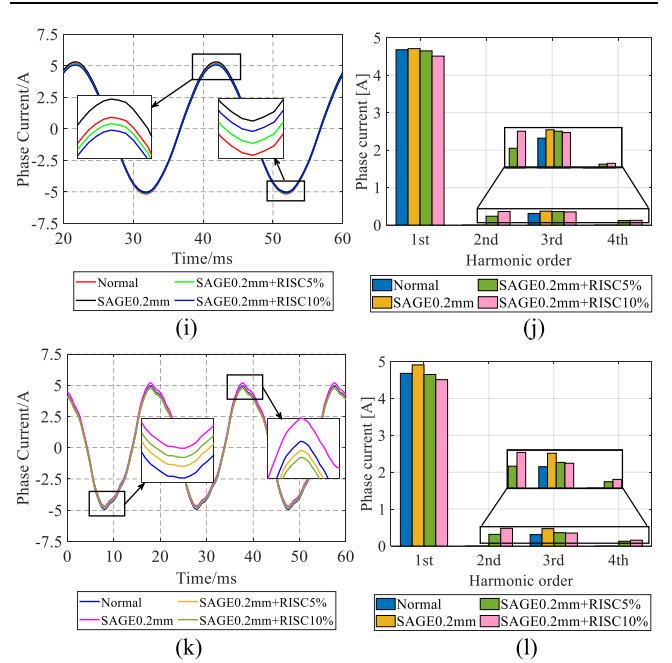


FIGURE 8 (Continued)

current of the motor decrease after the short circuit. Both odd and even harmonic components exist in the magnetic compact spectrum graph. Compared with normal conditions, the amplitude of the odd harmonic component and the even harmonic component increase when RISC occur. These results are consistent with the theoretical analysis conclusion of Figure 3 and Equation (8), which proves the correctness of the previous theoretical analysis results.

3.2.3 | MFD and current change after SAGE failure

The MFD and phase current changes caused by SAGE and RISC components under the compound fault are shown in Figure 8a,b,g,h.

As can be seen in Figure 8, the effect of MFD/stator current under the composite fault increases the RMS (effective value) and maximum harmonic of MFD/stator current, and the increase in the MFD/stator current curve shows a 'compression' effect, which will decrease the RMS and amplitude of the MFD/current, which is a consistent result in Figure 7.

Comparing Figure 8a,c,e and Figure 6a,c,e, with the equal eccentricity, the pass harmonic value of the MFD/current corresponding to the composite fault is reduced compared with the single fault of the SAGE. This is because the RISC component existing in the composite fault has the effect of reducing the MFD. Comparing Figure 8b,d,h and Figure 6b,d,h, the composite fault has more even harmonic components than a single SAGE fault; as the amount of eccentricity increases, the odd harmonic amplitude increases under both single SAGE and composite faults, and the increase

TABLE 2 Statistical table of key parameters under different working conditions

State	Harmonic							RMS	
	1st	2nd	3rd	4th	mean				
Normal	FEA	4.5	0	0.31	0	0	↓	3.621	–
	EXP	4.32	0	0.26	0	0		3.619	
SAGE 0.1 mm	FEA	4.61	0	0.38	0	0.12		3.621	
	EXP	4.51	0	0.32	0	0.126		3.622	
SAGE 0.2 mm	FEA	4.72	0	0.45	0	0.181		3.621	
	EXP	4.63	0	0.43	0	0.178		3.618	
RISC 5%	FEA	4.41	0.21	0.28	0.09	0	–	3.611	↑
	EXP	4.18	0.22	0.27	0.06	0		3.602	
RISC 10%	FEA	4.01	0.32	0.26	0.1	0		3.584	
	EXP	3.63	0.28	0.19	0.13	0		3.579	
RISC 10% + SAGE 0.1 mm	FEA	4.19	0.24	0.28	0.12	0.176	↓	3.584	–
	EXP	4.18	0.27	0.26	0.133	0.172		3.583	
RISC 10% + SAGE 0.2 mm	FEA	4.21	0.36	0.29	0.126	0.179		3.584	
	EXP	4.22	0.31	0.31	0.151	0.175		3.582	
SAGE 0.2 mm + RISC 5%	FEA	4.65	0.236	0.361	0.121	0.181	–	3.602	↑
	EXP	4.65	0.316	0.361	0.13	0.182		3.598	
SAGE 0.2 mm + RISC 10%	FEA	4.51	0.361	0.353	0.126	0.179		3.581	
	EXP	4.51	0.481	0.352	0.158	0.180		3.573	

of the odd harmonic under a single SAGE fault is greater than that of a composite fault. The even harmonic amplitude also shows an increasing trend under the composite fault. This result again affirms the conclusion of the previous theoretical analysis on the eccentric reduction of the air gap, see Figure 2 for more details.

Compared with Figure 8g,i,k and Figure 7a,c and 7e, it can be seen that under the same short circuit degree, the corresponding MFD/current harmonic value is larger than the single RISC, which is due to the composite fault SAGE component of the ‘translation’ MFD curve. Figure 8h,j,l,g and Figure 7b,d,h, with the increase of short circuit, the single RISC and odd harmonic increases, and the decrease of the odd harmonic, because this addition is for the MFD whole, so both odd harmonic or even harmonic will be added.

Due to the different installed capacity of generators, when SAGE and RISC occur, the variation of each harmonic component is different, but the overall trend is consistent with the results of theory and simulation. We introduced two parameters, which is mean and RMS, and performed quantitative analysis in the form of a table. As shown in Table 2.

4 | CONCLUSION

In this paper, a fault diagnosis model based on magnetic density is proposed to analyse the current characteristics of synchronous generator rotor turn-to-turn short circuit and air

gap eccentric single fault and composite fault. The model considers the influence of rotor inter-turn short circuit and air gap eccentricity on air gap magnetic density. The conclusions are as follows:

- (1) The SAGE will produce a ‘translation’ addition to the MFD curve, resulting in the increase of the absolute amplitude and effective value of the MFD and current, and the amplitude of each odd harmonic;
- (2) The RISC produces the ‘compression’ effect of the MFD curve, resulting in reducing the amplitude and effective value of the MFD and current, the amplitude of each odd harmonic, increasing the amplitude of each even harmonic, and the even harmonic amplitude of the even harmonic increases with the aggravation of the living road;
- (3) Under the same eccentricity, the MFD/current corresponding to pass harmonic and odd harmonic increase is less than that of the single air gap; under the same short circuit situation, the pass harmonic and odd harmonic amplitude corresponding to composite fault is less than the single RISC fault, but the even harmonic increase is greater than the single RISC fault.

The results can be used as a supplement to the existing fault diagnosis criterion system, help to enrich the criterion collection, and further improve the fault monitoring and diagnosis accuracy of the generator on the existing basis.

AUTHOR CONTRIBUTIONS

Conceptualisation: Yu-Ling He, Ming-Hao Qiu, Fu-Cheng Zhou. Methodology: Yu-Ling He, Ming-Hao Qiu, Fu-Cheng Zhou. Software: Yu-Ling He, Ming-Hao Qiu, David Gerada. Validation: Pei-Jie Yang, Ming-Hao Qiu, Fu-Cheng Zhou. Formal analysis: Yu-Ling He. Investigation: Yu-Ling He, Ming-Hao Qiu, Fu-Cheng Zhou. Resources: Yu-Ling He, Ming-Hao Qiu, Fu-Cheng Zhou. Data curation: Yu-Ling He, Ming-Hao Qiu, Meng-Ya Jiang, Xiao-Chen Zhang, Xiao-Dong Du, Fu-Cheng Zhou. Writing – original draft preparation: Yu-Ling He, Ming-Hao Qiu. Writing – review and editing: Yu-Ling He, Ming-Hao Qiu. Supervision: Yu-Ling He, David Gerada. Project administration: Yu-Ling He, Ming-Hao Qiu. Funding acquisition: Yu-Ling He. All authors have read and agreed to the published version of the manuscript.

ACKNOWLEDGEMENTS

This work was supported in part by the National Natural Science Foundation of China (52177042), National Natural Science Foundation of China (51777074).

CONFLICT OF INTEREST

There are no conflicts of interest.

DATA AVAILABILITY STATEMENT

Data sharing not applicable to this article as no datasets were generated or analysed during the current study.

ORCID

Yu-Ling He  <https://orcid.org/0000-0003-2719-8128>

REFERENCES

- Hsieh, M.-Fu, Yeh, Yu-H.: Rotor eccentricity effect on cogging torque of PM generators for small wind turbines. *IEEE Trans. Magn.* 49(5), 1897–1900 (2013). <https://doi.org/10.1109/tmag.2012.2237021>
- David, G.: Dorrell and ahmad salah, detection of rotor eccentricity in wound rotor induction machines using Pole-specific search coils. *IEEE Trans. Magn.* 51(11), 18111604–4 (2015). <https://doi.org/10.1109/tmag.2015.2443711>
- Thomson, W.T., Barbour, A.: On-line current monitoring and application of a finite element method to predict the level of static airgap eccentricity in three-phase induction motors. *IEEE Trans. Energy Convers.* 13(4), 347–357 (1998). <https://doi.org/10.1109/60.736320>
- Faiz, J., Moosavi, S.M.M.: Review of eccentricity fault detection techniques in IMs focusing on DFIG. In: 2015 IEEE 5th International Conference on Power Engineering, Energy and Electrical Drives (POWERENG), pp. 513–520 (2015)
- Hyun, D., et al.: Detection of airgap eccentricity for induction motors using the single-phase rotation test. *IEEE Trans. Energy Convers.* 27(3), 689–696 (2012). <https://doi.org/10.1109/tec.2012.2198218>
- Dorrell, D.G., Salah, A., Guo, Y.: The detection and suppression of unbalanced magnetic pull in wound rotor induction motors using Pole-specific search coils and auxiliary windings. *IEEE Trans. Ind. Appl.* 53(3), 2066–2076 (2017). <https://doi.org/10.1109/tia.2017.2672748>
- Belachen, A., Arkkio, A.: Computation of additional losses due to rotor eccentricity in electrical machines. In: *IET Electric Power Applications*. 4(4), 259–266 (2010)
- Guerrero, J.H.C., Salinas, D.O.: Experimental analysis of eccentricity in salient-pole synchronous machines. Part I: prototype design, construction and tests. In: 2010 International Conference on Advances in Energy Engineering, pp. 5–8 (2010)
- Hsieh, M.-Fu, Yeh, Yu-H.: Rotor eccentricity effect on cogging torque of PM generators for small wind turbines. *IEEE Trans. Magn.* 49(5), 1897–1900 (2013). <https://doi.org/10.1109/tmag.2012.2237021>
- Ilamparithi, T., Nandi, S.: Analysis, modeling and simulation of static eccentric reluctance synchronous motor. In: 2011 IEEE International Symposium on Diagnostics for Electric Machines, Power Electronics & Drives, pp. 45–50 (2011)
- Tenhunen, A.: Calculation of eccentricity harmonics of the air-gap flux density in induction Machines by impulse method. *IEEE Trans. Magn.* 41(5), 1904–1907 (2005). <https://doi.org/10.1109/tmag.2005.846254>
- Wang, L., et al.: Finite-element analysis of unbalanced magnetic pull in a large hydro-generator under practical operations. *IEEE Trans. Magn.* 44(6), 1558–1561 (2008). <https://doi.org/10.1109/tmag.2007.916023>
- Zarko, D., et al.: Calculation of unbalanced magnetic pull in a salient-Pole synchronous generator using finite-element method and measured shaft orbit. *IEEE Trans. Ind. Electron.* 59(6), 2536–2549 (2012). <https://doi.org/10.1109/tie.2011.2160515>
- Climente-Alarcon, V., et al.: Transient tracking of low and high-order eccentricity-related components in induction motors via TFD tools. *Mech. Syst. Signal Process.* 25(2), 667–679 (2011). <https://doi.org/10.1016/j.ymssp.2010.08.008>
- Cameron, A.W.W.: Diagnoses of A-C generator insulation condition by nondestructive tests includes discussion. *Power Apparatus Syst. Part III Trans. Am. Inst. Electr. Eng.* 71(1), 263–269 (1952). <https://doi.org/10.1109/aiecpas.1952.4498471>
- Hang, J., et al.: Detection of interturn short-circuit fault for PMSM with simple fault indicator. *IEEE Trans. Energy Convers.* 31(4), 1697–1699 (2016). <https://doi.org/10.1109/tec.2016.2583780>
- Park, Y., et al.: Influence of blade pass frequency vibrations on MCSA-based rotor fault detection of induction motors. In: *IEEE Transactions on Industry Applications*. 53(3), 2049–2058 (2017)
- Albright, D.R.: Interturn short-circuit detector for turbine-generator rotor windings. *IEEE Trans. Power Apparatus Syst.* PAS-90(2), 478–483 (1971). <https://doi.org/10.1109/tpas.1971.293048>
- Cuevas, M., et al.: Non-invasive detection of rotor short-circuit fault in synchronous machines by analysis of stray magnetic field and frame vibrations. *IEEE Trans. Magn.* 52(7), 1–4 (2016). <https://doi.org/10.1109/tmag.2016.2514406>
- He, Y.-L., et al.: A novel universal model considering SAGE for MFD-based faulty property analysis under RISC in synchronous generators. In: *IEEE Transactions on Industrial Electronics*. 69(7), 7415–7427 (2022). <https://doi.org/10.1109/TIE.2021.3094481>
- Hao, L., et al.: Steady-state calculation and online monitoring of interturn short circuit of field windings in synchronous machines. *IEEE Trans. Energy Convers.* 27(1), 128–138 (2012). <https://doi.org/10.1109/tec.2011.2169264>
- Li, G.J., et al.: Excitation winding short-circuits in hybrid excitation permanent magnet motor. *IEEE Trans. Energy Convers.* 29(3), 567–575 (2014). <https://doi.org/10.1109/tec.2014.2322194>
- Wan, S., et al.: Investigation on stator circulating current characteristics of turbogenerators under air gap eccentricity rotor and short-circuit composite faults. *Elec. Power Compon. Syst.* 38(8), 900–17 (2010). <https://doi.org/10.1080/15325000903571525>
- Sinervo, A., Arkkio, A.: Eccentricity related forces in two-Pole induction motor with four-Pole stator damper winding analyzed using measured rotor orbits. *IEEE Trans. Magn.* 49(6), 3029–3037 (2013). <https://doi.org/10.1109/tmag.2013.2238637>
- Sinervo, A., Laiho, A., Arkkio, A.: Low-frequency oscillation in rotor vibration of a two-Pole induction machine with extra four-Pole stator winding. *IEEE Trans. Magn.* 47(9), 2292–2302 (2011). <https://doi.org/10.1109/tmag.2011.2142007>
- He, Y., et al.: A new hybrid model for electromechanical characteristic analysis under SISC in synchronous generators. *IEEE Trans. Ind. Electron.* 67(3), 2348–2359 (2020)

27. Hao, L., et al.: Diagnosis of rotor winding short-circuit fault in multi-phase Annular brushless exciter through stator field current harmonics. In: IEEE Transactions on Energy Conversion. 36(3), 1808–1817 (2021). <https://doi.org/10.1109/TEC.2021.3058279>
28. Liang, F., et al.: Fault Diagnosis of inter-turn short circuit in rotor winding of doubly-fed generator based on data fusion of multi-flux sensors. In: 2021 International Conference on Sensing, Measurement & Data Analytics in the Era of Artificial Intelligence (ICSMD), pp. 1–4 (2021). <https://doi.org/10.1109/ICSMD53520.2021.9670827>

How to cite this article: He, Y.-L., et al.: Stator current identification in generator among single and composite faults composed by static air-gap eccentricity and rotor inter-turn short circuit. IET Electr. Power Appl. 1–11 (2022). <https://doi.org/10.1049/elp2.12260>